4th International Conference on
Earthquake Geotechnical Engineering
June 25-28, 2007
Paper No. 1346

AN ENERGY BASED EXCESS PORE PRESSURE GENERATION MODEL UNDER EARTHQUAKE LOADING

S.I. Kim[1], K.B. Park[2], S.Y. Park[3], B.K. Kim[4], and I.J. Park[5]

ABSTRACT

The main objective of this paper is to develop an improved method for the analysis of liquefaction potential and to predict excess pore pressure (EPP) using the proposed model that can simulate behavior of saturated sand under irregular dynamic loading conditions. The EPP generation model is developed through empirical analysis. For the development of the model, a general formulation based on experimental results and integral method using cumulative absolute velocity (CAV) weight function is proposed for a more realistic description of dynamic responses of saturated sand. The motivation for the development of an energy-based model is for application to projects and problems involving liquefaction for soil under earthquake type loading. This paper presents the basic theory and verification of the proposed model based on results from dynamic triaxial tests for saturated sand with various earthquake type loadings.

Keywords: dissipated energy, excess pore pressure generation model, cumulative absolute velocity, dynamic triaxial test, earthquake type loading, initial liquefaction

INTRODUCTION

For the evaluation of liquefaction potential or susceptibility for sands, experimental investigations are often used based on cyclic triaxial tests or in-situ field tests, called the stress- (Seed and Idriss 1971) and the strain-based method (Dobry et al. 1982). Although these methods have been widely used in practice, those are essentially simplified approaches since no detailed behavior including the actual loading conditions, duration of excitation, and mobilization of the EPP can be explained (Tao 2003).

In addition to the stress- and the strain-based method, numerous energy-based EPP generation models (Nemat-nasser and Shokooh 1979; Simcock et al. 1983; Law et al. 1990; Green et al. 2000) have been developed. According to Law et al. (1990), Liang et al. (1995), and Green (2001), energy based procedure for liquefaction analysis has several advantages compared with the stress and strain-based method.

Nemat-Nasser and Shokooh (1979) developed a relatively simple theory that related soil densification and pore pressure generation to dissipated energy. Others (Simcock et al. 1983; Law et al. 1990; Green et al. 2000) have since attempted to characterize the relationship between EPP and dissipated energy experimentally. While EPP generation models have been successfully verified for many geotechnical dynamic problems, these models have been primarily for cyclic loading test results. For the liquefaction analysis, it is known that the sinusoidal type of cyclic loading does not realistically

[1] Professor, Department of Civil Engineering, University of Yonsei, Korea, Email: geotech@yonsei.ac.kr
[2] Graduate Student, Department of Civil & Environmental Engineering, University of Yonsei.
[3] Graduate Student, Department of Civil & Environmental Engineering, University of Yonsei.
[4] Graduate Student, Department of Civil & Environmental Engineering, University of Yonsei.
[5] Professor, Department of Civil Engineering, Hanseo University, Korea

represent actual irregular earthquake loadings (Ishihara and Yasuda 1972; Kim et al. 2005). Therefore, effects of the actual irregular earthquake loadings should also be taken into account for more detailed and advanced liquefaction analysis.

In this study, an EPP generation model for the prediction of EPP and the identification of liquefaction potential for sand subjected to irregular loading is developed through empirical and analytical investigations based on the EPP and the dissipated energy. For more realistic description of dynamic responses of saturated sands, a new EPP generation model is proposed based on empirical results and integral method using CAV. To predict EPP using the proposed model, dynamic tests are performed. Based on test results, mobilization of the EPP and the dissipated energy are analyzed and compared. The convenient initial liquefaction criterion is addressed for various loading types. The calibration parameters are determined through relationship of the calibration parameters and initial liquefaction from laboratory test results. A prediction procedure of the liquefaction initiation and the EPP is proposed. Results from the independent test are compared with numerical results obtained from the proposed model.

GENERAL EPP GENERATION MODEL AND EARTHQUAKE INTENSITY

General energy-based excess pore pressure generation model

When dynamic loadings are propagated through soil, soil will deform in a hysteretic manner and a portion of their energy will be dissipated. During this deformation process, the dissipated energy can be commonly represented by the area of the hysteresis loop given in the stress-strain curve under dynamic loading conditions. The expression for dissipated energy is given by:

$$w_d(t) = \int_0^t \sigma d\varepsilon^p \approx \sum_{i=1}^{t} \sigma_i d\varepsilon_i^p \tag{1}$$

where, σ = applied stress; $d\varepsilon^p$ = plastic strain; t = time; and i denotes the number of increments or cycle.

If sand is saturated and drainage is not permitted, an increase in the EPP results from the volume change. An EPP is then generated as proposed by Law et al. (1990).

$$\Delta u = E_r \cdot F(w) \tag{2}$$

where, E_r = modulus of resilience; and $F(w)$ = function of dissipated energy. This EPP generation models provide credence to quantifying soil capacity in terms of dissipated energy. Thus, the development of EPP and the occurrence of liquefaction are related to the amount of energy dissipated in the soil.

Cumulative absolute velocity

The destructiveness of a seismic excitation cannot always be described by the peak ground acceleration (PGA) alone, or other seismic parameter such as peak ground velocity and displacement. Recently, the damage potential of the seismic excitation correlates better with kinetic energy based descriptors (Meskouris et al. 1993; Elenas and Liolios 1995) such as ARIAS intensities (Arias 1970), energy response spectra, strong motion duration values (Trifunac and Novikova 1994). Specially, CAV (Kramer and Mitchell 2006) to evaluate the liquefaction potential have received great interests because these approaches provide more detailed prediction of the performance of soil-structure systems and soil liquefaction. The CAV is measured from the total energy content of a seismic excitation and is defined by the following relation

$$CAV = \sum_{i=1}^{t} |a(t)|_i = \frac{A}{m} \cdot \sum_{i=1}^{t} |\sigma(t)|_i \quad (3)$$

where, t = time; $a(t)$ = the ground acceleration; A = area of soil sample; m = mass; and $\sigma(t)$ = applied stress. CAV is called scalar function. It is directly quantifiable through the acceleration record or stress, integrating it over the total duration of the earthquake. Unlike PGA, it considers the full range of frequencies recorded and included in the acceleration and the duration of the ground motion.

LABORATORY INVESTIGATION OF DYNAMIC RESPONSE AND DISSIPATED ENERGY

Dynamic triaxial test

To investigate dynamic responses and dissipated energy of saturated sand, dynamic undrained triaxial tests were performed by using irregular earthquake loading types. For the tests, 11 acceleration records were selected from recent major earthquakes of magnitudes between 6.2 and 8.2. The significant duration is 5-95% RMS (Root-Mean-Square) duration (Abrahmson & Silva 1996). Values of significant durations for earthquakes used in this study are 8 to 24 sec. The time history of acceleration obtained from Ormond earthquake is shown in Figure 1. Because there is a proportional relation between the deviatoric stress acting on a soil element at a certain depth and the acceleration (Seed and Idriss 1971; Ishihara and Yasuda 1972 and 1975), this pattern of time history was used for the voltage output from the computer through a digital to analog converter. The voltage through the actuator is converted into the deviatoric stress. Applying each of these load patterns (voltage) with the same speed as actually recorded in accelerations, a series of triaxial tests was performed for test procedures as described in Ishihara and Yasuda (1972). To evaluate the maximum deviatoric stress at which liquefaction first generated under irregular earthquake loadings, following steps were proceeded. At the first step, the test was carried out using an appropriate deviatoric stress level, which was small enough not to cause liquefaction. In the next step, the level of the deviatoric stress was increased slightly with the same wave form as used in the previous step. After repeating this procedure, liquefaction eventually occurred showing the induced EPP equal to the confining pressure. The deviatoric stress at this point is defined as the maximum deviatoric stress for a given earthquake types.

Test soil was the Jumunjin sand, the representative clean silica sand in Korea with properties given in Table 1. Triaxial soil samples tested in this study are of 70 mm in diameter and 135 mm in height. The moist tamping method (or moist placement method) (Ladd 1978; Vasquez-Herrera and Dobry 1989) was utilized for sample preparation. All the tests were carried out at isotropically consolidated conditions with a confining pressure level equal to 100 kPa and relative density of 60 %. When the B parameter reached a value greater than 0.98, the confining pressure was applied.

Table 1. Basic properties of Jumunjin sand

γ_{dmax} (kN/m^3)	γ_{dmin} (kN/m^3)	e_{max}	e_{min}	G_S	D_{50} (mm)	C_u *	C_c **
15.7	13.6	0.719	0.625	2.63	0.52	1.35	1.14

C_u * = coefficient of uniformity, C_c ** = coefficient of curvature.

Dynamic responses under irregular loadings

Test results with the irregular earthquake loading tests are shown in Figure 1. The test results appear to be quite different from those for general sinusoidal loading cases. Figure 1(a) shows the response time history of the resistant deviatoric stress and EPP for Ormond earthquake loading case. As indicated in Figure 1(a), it is seen that the EPP does not increase in earlier stages, but suddenly jumps up when the maximum deviatoric stress is reached, whereupon liquefaction sets in. Figure 1(b) shows the hysteresis loops. Differently from the sinusoidal loading test results, the loops for the earthquake loading tend to become progressively flatter as the sample begins to liquefy. The same phenomena were observed for

other earthquake loadings. After liquefaction, they are almost horizontal and their areas near zero indicating that the dissipated energy ceases to increase.

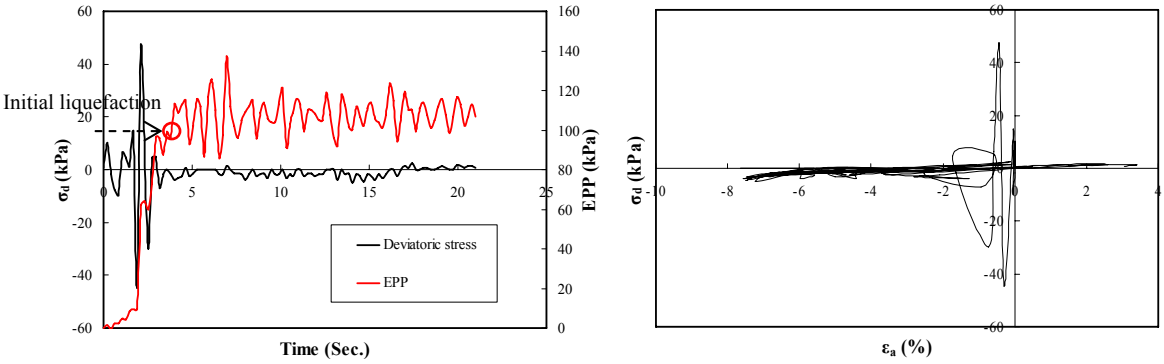

(a) Deviatoric stress and EPP versus time **(b) Stress-strain curves**

Figure 1. Test results for earthquake loading (Ormond, M_W=6.2, 1993), σ_{dmax} = 46 kPa

Dissipated energy versus excess pore pressure

To compare liquefaction initiation procedure for earthquake loadings, relationships of dissipated energy (w_d(t)) versus EPP ratio were plotted in Figure 2. In this figure, the EPP has been nondimensionalized by the confining pressure used for the test called EPP ratio. Dissipated energy for each cycle was obtained from the stress-strain curve using Equation (1).

Figure 2 shows test results for earthquake loadings until initial liquefaction. Since stresses and strains are remarkably unsystematic for earthquake loadings, EPP versus w_d(t) curves using Equation (2) appear to be also of irregular shape. As indicated in Figure 2, the extent of scatter is fairly severe and no unique correlation appears to be obtained. This result indicates that further investigation is still needed for practically feasible application of the energy based approach.

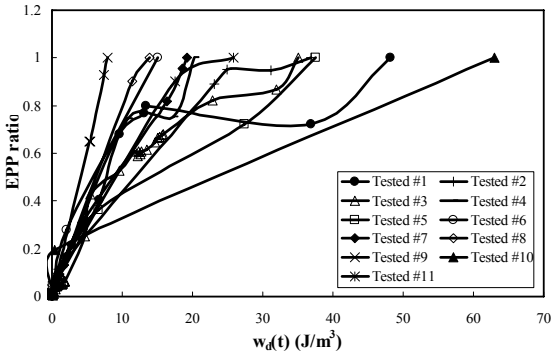

Figure 2. Test results for dissipated energy and EPP ratio

LIQUEFACTION ANALYSIS BASED ON EPP GENERATION MODEL

Damage process

Consider a damaged specimen loaded by earthquake loading. The earthquake stress can be divided into two parts: the regular stress which appears under the loading conditions in the undamaged zone, and a corrective stress due to the presence of the damage zone. Note that the corrective stress is generated by the CAV induced by the earthquake loading. Therefore, the earthquake stress for the problem can be calculated from the summation for these two parts

$$CS^t = CS^{damage} + CS^{undamage} = CS^t \cdot d_{CAV} + CS^t \cdot \left(1 - d_{CAV}\right) \tag{4}$$

where, CS^t = given stress; CS^{damage} = stress for damage; $CS^{undamage}$ = stress for undamaged; and d_{CAV} = CAV weight function. To describe the stress in terms of damage potential, the stress acting on the damaged and undamaged zone is calculated to be CAV, as CAV is strength of shaking produced by an earthquake and function of the degree of damage potential. Accordingly, stresses in the undamaged soil element can be defined as follows:

$$CS^{undamage} = CS^t - CS^{damage} = CS^t \cdot \left(1 - d_{CAV}\right) \tag{5}$$

During earthquake, geometrical damage potential (changes in the geometry of the soil owing to CAV) for given soil result in a reduction in both stiffness and strength. The reduced soil strength ratio is set equal to the value of the strength ratio for shaking produced by the earthquake. The CAV weight function is in turn defined as a function of the acceleration time history or stress time loading history. Thus, CAV weight function is as follow

$$d_{CAV} = \frac{CAV}{CAV_{\max}} = \frac{\frac{A}{m} \cdot \sum_{i=1}^{t} \left|\sigma(t)\right|_i}{\frac{A}{m} \cdot \sum_{i=1}^{t_{\max}} \left|\sigma(t)\right|_i} \tag{6}$$

where, $CAV_{\max} = CAV$ until the end of the loading cycle; A = area; m = mass; $\sigma(t)$ = applied stress; t = time; and $t_{\max}$ = time until the end of the loading cycle. The CAV weight function term d_{CAV}, has the limits $0 \leq d_{CAV} \leq 1.0$. The condition $d_{CAV} = 0$ defines a material state wherein there is no damage, which exists prior to the onset of any loading; the condition $d_{CAV} = 1.0$ defines a state of perfect failure in the material.

Liquefaction is a damage potential process in which EPP develops incrementally as increasing stress reversals takes place. EPP may also increase in critically stressed areas during earthquakes to produce failure (Kramer et al. 2002). If the stress is applied to a saturated soil specimen, the soil system changes with EPP; consequently, the EPP changes with damage potential. EPP acting on the damaged zone is assumed to consist of two zones: the damaged and undamaged zones. With incremental increases in EPP, the damaged zone increases in extent whereas the undamaged zone decreases. If the concentration of EPP is assumed to reflect the distribution of the damage potential, EPP components for the damage element can be defined as follows:

$$u = u^{damage} + u^{undamage} = d_{CAV} \cdot u + \left(1 - d_{CAV}\right) \cdot u \tag{7}$$

where, u = EPP; u^{damage} = EPP for the damaged zone; and $u^{undamage}$ = EPP for the undamaged zone.

Cumulative stress, excess pore pressure, macroscopic dissipated energy

To consider the entire wave form, including amplitude and duration, integration of both sides for Equation (5) gives

$$CP^u = \sum_{i=1}^{t} \left(CS^t\right)_i \cdot \left(1 - d_{CAV}\right)_i \tag{8}$$

where, CP^u = cumulative stress for undamaged zone; and i denotes the number of increments or cycle. Similar to Equation (8), integration of both sides for Equation (7) gives

$$CEP = \sum_{i=1}^{t} u_i \cdot \left(1 - d_{CAV}\right)_i \tag{9}$$

where, CEP = cumulative EPP for undamaged zone. In terms of the EPP ratio (i.e., ratio of EPP to the confining pressure), Equation (9) can be rewritten as follows:

$$r^a = \sum_{i=1}^{t} \left(r^t\right)_i \cdot \left(1 - d_{CAV}\right)_i \tag{10}$$

where, r^a = cumulative EPP; and r^t = EPP ratio.

To compare with cumulative stress, a macroscopic dissipated energy similar to integral of Equations (8) and (10) is addressed as follows:

$$W = \sum_{i=1}^{t} w_d(t)_i \tag{11}$$

where, W = macroscopic dissipated energy; and $w_d(t)$ = dissipated energy.

It is evident from Figure 2 that a simple, unique relationship between EPP and $w_d(t)$ does not appear for the Jumunjin sand tested in this study. It is possible, however, to conjecture on the existence of a relationship between EPP, $w_d(t)$, and deviatoric stress. In Figure 3, we have replotted the data from Figure 2 but with deviatoric stress, EPP, and w_d(t) values scaled by Equation (8), (10), and (11). In Figure 3, CP^u and r^a denotes cumulative stress and cumulative EPP, respectively. As shown in Figure 3, systematic curves are observed better than those curves in Figure 2. Figure 3 (a) shows the cumulative stress curves as a function of macroscopic dissipated energy, observed in the triaxial test results. Figure 3 (b) shows the cumulative EPP curves which were calculated by integrating the value of every cumulative EPP increment. In Figure 3, all of the cumulative stress and the cumulative EPP increase took place during the point at which the macroscopic dissipated energy reaches some value and then its value maintained till the end of test. To normalize the correlation shown in Figure 3, we defined the following normalized values

$$Nor\ CP^u = \frac{CP^u}{CP^u{}_{\max}} \tag{12}$$

$$Nor\ r^a = \frac{r^a}{r^a{}_{\max}} \tag{13}$$

$$Nor\ W = \frac{W}{W_{\max}} \tag{14}$$

where, $Nor\ CP^u$, $Nor\ r^a$, and $Nor\ W$ = normalized cumulative stress, cumulative EPP, and macroscopic dissipated energy ratio, respectively; and CP^u, $r^a{}_{\max}$, and $W_{\max}$ = maximum cumulative stress, cumulative EPP ratio, and macroscopic dissipated energy at the end of the loading cycle, respectively.

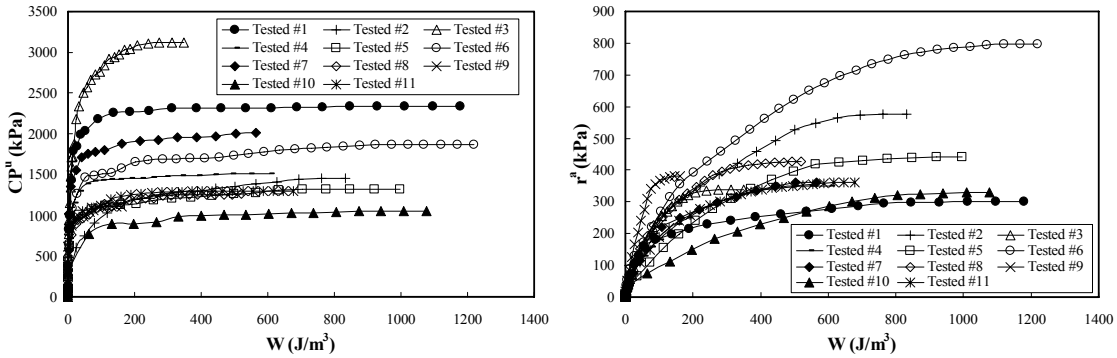

(a) CP^u curves **(b) r^a curves**

Figure 3. Test results of the cumulative stress curves and the cumulative EPP curves

Figure 4 shows values of *Nor* CP^u and *Nor* r^a plotted against *Nor W* for the earthquake loading cases. All of the trends show distinct relationships between the plotted variables, indicating that normalized r^a and W can be effectively used in estimating EPP generation.

From Figure 4, it is seen that curves of *Nor* r^a and the *Nor* CP^u with *Nor W* can be approximated by a simple exponential function. Therefore, it can be expressed as follows:

$$Nor\ r^a = 1 - \exp(-A_r\ Nor\ W^{Z_r}) \tag{15}$$

$$Nor\ CP^u = 1 - \exp(-A_W\ Nor\ W^{Z_W}) \tag{16}$$

where, A_W , A_r , Z_W , and Z_r = calibration parameters obtained from experimental test results. These functions used in the current study are similar to the Weibull function (Weibull 1951), commonly used for growth and decay processes.

The calibration parameters A_W , A_r , Z_W , and Z_r control the rate and shape of the *Nor* CP^u and *Nor* r^a curves. To determine A_r and Z_r , once *Nor* CP^u and *Nor W* are known for each cycle, $\ln\left[-\ln\left\{\left(1 - Nor\ r^a\right)\right\}\right]$ versus $\ln$ *Nor W* is plotted. One can determine the best fit line to the set of points $\left(\ln\left[-\ln\left\{\left(1 - Nor\ r^a\right)\right\}\right], \ln Nor\ W\right)$ to evaluate A_r and Z_r . The values of the intercept and the slope of the average line represents $\ln A_r$ and Z_r , respectively. The calibration parameters A_W and Z_W can also be found by same procedure.

Nor r^a and *Nor* CP^u function can be defined with respect to *Nor W*. *Nor* r^a , *Nor* CP^u , and *Nor W* can be calculated for each cycle by using Equations (12), (13), and (14) normalizing Equations (8), (10), and (11), respectively. Figure 4 shows tested and calculated *Nor* r^a and *Nor* CP^u using Equations (15) and (16). By comparing Figure 4, we can find the tested results can be successfully simulated using Equations (15) and (16).

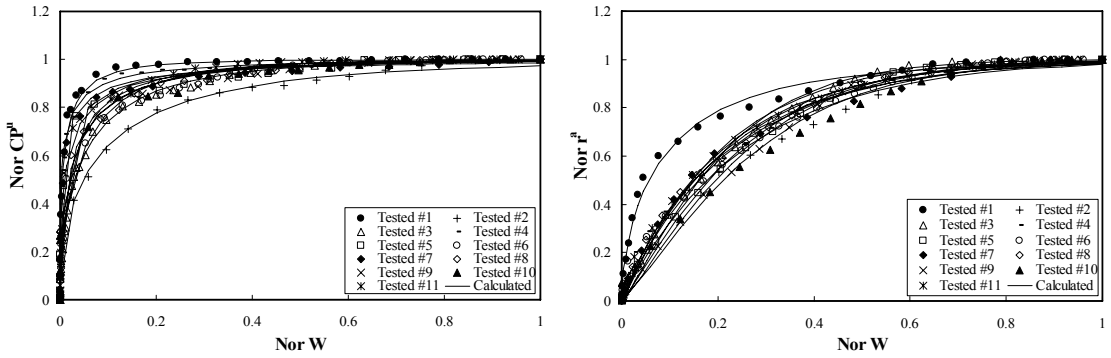

(a) Normalized CP^u ratio curves **(b) Normalized r^a curves**

Figure 4. Tested and calculated results of the normalized cumulative stress ratio curves and the normalized cumulative EPP ratio curves

Energy based excess pore pressure generation model

The normalized EPP can be derived as the following equation by differentiating Equation (15) with respect to $NorW$.

$$\frac{d\,Nor\,r^a}{d\,Nor\,W} = \frac{Nor\ r^a{}_i - Nor\ r^a{}_{i-1}}{Nor\ W_i - Nor\ W_{i-1}} = \left(A_r \cdot Z_r\right) \cdot NorW^{Z_r - 1} \cdot \exp\left(-A_r \cdot NorW^{Z_r}\right) = K \tag{17}$$

Substitution for $Nor\ r^a$ from relation given in Equation (13) and (14) into Equation (17) yields

$$\frac{d\,Nor\,r^a}{d\,Nor\,W} \cdot \left(\frac{r^a{}_{\max}}{W_{\max}}\right) = K \cdot \left(\frac{r^a{}_{\max}}{W_{\max}}\right) = \frac{r^t \cdot (1 - d_{CAV})}{w_d} \tag{18}$$

where, r^t = EPP ratio; and w_d = dissipated energy. Therefore, the EPP ratio yields

$$r^t = K \cdot \left(\frac{w_d}{1 - d_{CAV}}\right) \cdot \left(\frac{r^a{}_{\max}}{W_{\max}}\right) = R^t \cdot r^a{}_{\max} \tag{19}$$

where, R^t = EPP shape function.

To calculate $r^a{}_{\max}$ in attempting to determine EPP ratio based on only the input loading, it is necessary to know the EPP ratio throughout the entire loading cycle; however, if we are able to determine the initial liquefaction, $r^a{}_{\max}$ can be calculated because the EPP ratio is 1 following the initial liquefaction. Accordingly, the R^t in Equation (19) is normalized as the value of the EPP shape function at the initial liquefaction, $r^a{}_{\max}$ can be rewritten as follows:

$$r^a{}_{\max} = \sum_{i=1}^{t_{\max}} \left(\frac{R^t}{R_{ini}}\right)_i \tag{20}$$

where, R_{ini} = R^t value at the initial liquefaction; and $t_{\max}$ = time until the end of the loading cycle. The method used to determine the initial liquefaction is explained in the following section.

LIQUEFACTION INITIATION AND PREDICTION OF EXCESS PORE PRESSURE

Critical cumulative stress and identification of initial liquefaction

Figure 4 shows that there are specific locations where significant slope changes occurs in $Nor\ CP^u$ curve. This change of $Nor\ CP^u$ is related to the transformation of the threshold into failure state (here, failure is assumed as the end of the test). During dynamic loading, change of instabilities in the microstructure of the material can be represented by the $Nor\ CP^u$ in Equation (16). From the $Nor\ CP^u$ curve in Figure 4, it is seen that there is a point of the maximum curvature before the stabilized $Nor\ CP^u$ value equal to 1 is reached. Value of $Nor\ CP^u$ corresponding to this point is defined as the critical cumulative stress $Nor\ CP_c^u$. The state of $Nor\ CP_c^u$ at which some material under certain load reaches can indicate a state of instability threshold that can identify initial liquefaction. To find $Nor\ CP_c^u$, the maximum curvature equation is defined as (Park 1997)

$$R = \frac{\left(Nor\ CP^u\right)''}{\left(1+\left(Nor\ CP^u\right)'^2\right)^{3/2}} \tag{21}$$

where, R = curvature of $Nor\ CP_c^u$ function curve given by Equation (16); and $\left(Nor\ CP^u\right)'$ and $\left(Nor\ CP^u\right)''$ = the first and second derivatives of the $Nor\ CP_c^u$ with respect to *Nor W*.

In calculated results, it can be seen that the number of cycles (N_c) = 5 corresponding to $Nor\ CP_c^u$ = 0.8171 for Ormond (#5) loading compare well with that (N_c = 5) measured in the laboratory tests. The other loading test results are shown in Table 2. As shown in Table 2, the N_c corresponding to $Nor\ CP_c^r$ obtained from this procedure shows an excellent match with the number of cycles (N_{liq}) causing liquefaction in laboratory tests.

Table 2. Comparison between tested and calculated number of cycles to initial liquefaction

Earthquake, year	Tested Number	Critical cumulative power	Tested initial liquefaction (N_c)	Calculated initial liquefaction (N_{liq})
Cass, 1995	#1	0.9355	11	11
El Centro, 1940	#2	0.6494	6	6
Taumaranui, 1973	#3	0.8424	36	27
Costa Rica, 1991	#4	0.8859	9	9
Ormond, 1993	#5	0.8171	5	5
Parkfield, 1966	#6	0.7546	6	7
Coalinga, 1983	#7	0.8432	7	7
Hachinohe, 1968	#8	0.8002	8	10
Kamitsuki, 2000	#9	0.8566	12	12
Loma Pieta, 1989	#10	0.8159	7	8
Ofunato, 1978	#11	0.8566	6	8

Prediction procedure of excess pore pressure using proposed Model

The proposed model that is commonly available to practicing geotechnical engineers set a few calibration parameters such as A_r , and Z_r . The proposed procedure can provide an EPP generation model that can represent the actual behavior of liquefiable soils under earthquake loading. It also calculates the pore pressure buildup using only input loading. In this procedure, an increment stress is

given as input data. Once $d\varepsilon$ are evaluated, the dissipated energy can be calculated using Equation (1). In the present study, the method proposed by Kim (2003) was used for the numerical integration procedure to obtain the strain value.

After the values of W and d_i are found in prediction procedure, $Nor\ CP^u$ versus $Nor\ W$ plots are obtained for various loading types and then A_W , Z_W are determined. We need value of κ_f corresponding to initial liquefaction to determine A_r and Z_r . Relationship of κ_f, A_r , and Z_r is described in the following section.

Determination of calibration parameters (A_r and Z_r)

For determination of calibration parameters A_r and Z_r , we adopted the stress damage ratio (Kim et al. 2005). According to Kim et al. (2005), it was concluded that the κ can be used as an effective parameter of the classification for type of dynamic loadings. New stress-time history parameters, κ and κ_f are introduced and defined as follows:

$$\kappa = \frac{1}{t_{\max} \cdot \sigma_{d\max}} \left(\sum_{0}^{t_{\max}} |\sigma_d \cdot t| \right) \tag{22}$$

where, $\sigma_{d\max}$ = maximum deviatoric stress; σ_d = deviatoric stress; $t_{\max}$ = time until the end of the test; and t = time. The summation in Equation (22) represents the entire areas until the end of the test. κ_f represents the value of κ for summation of stress-time history curve until the liquefaction initiation. To determine A_r and Z_r , it is necessary to find liquefaction initiation using Equation (16) and (21). After evaluating initial liquefaction from all test results, κ_f is obtained through comparison between κ value and liquefaction initiation point. Figure 5 shows results for the A_r and Z_r developed by irregular earthquake loadings for κ_f values. It is observed in Figure 5 that the calibration parameters A_r and Z_r increase with increasing κ_f values. A_r and Z_r were found to be linearly dependent value on the κ_f. These functions are given by:

$$A_r = 32.556 \cdot \kappa_f + 2.4510 \tag{23}$$

$$Z_r = 4.7065 \cdot \kappa_f + 0.6811 \tag{24}$$

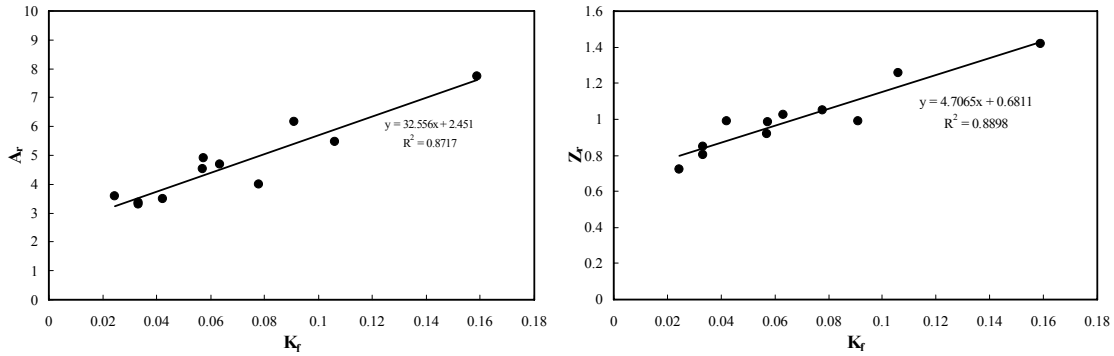

(a) A_r curves **(b) Z_r curves**

Figure 5. Evaluation of the calibration parameters A_r and Z_r for the experimental response

Prediction of excess pore pressure using independent test results

To verify the proposed EPP model developed in this study, two earthquake type loadings triaxial tests were performed additionally. The soil sample was the Jumunjin sand as used in previous tests. Figure

6 shows tested and predicted behavior of saturated sand with D_r = 60% and confining pressure = 100 kPa under earthquake type loads. Tests shown in Figure 6 are the tests which are not used for the determination of parameters. The calibration parameters A_r and Z_r are determined from Equation (23) to (24).

To determine initial liquefaction, $Nor\ CP_c^u$ is calculated by using Equation (21). Figure 6 shows the comparison between tested and calculated rate of EPP with time (or N_c). Here, the EPP is computed by using Equation (19). As shown in the figure, the proposed model represents the tested EPP generation behavior very well. Especially, the proposed model provides highly satisfactory EPP generation results in samples subjected to irregular earthquake loadings.

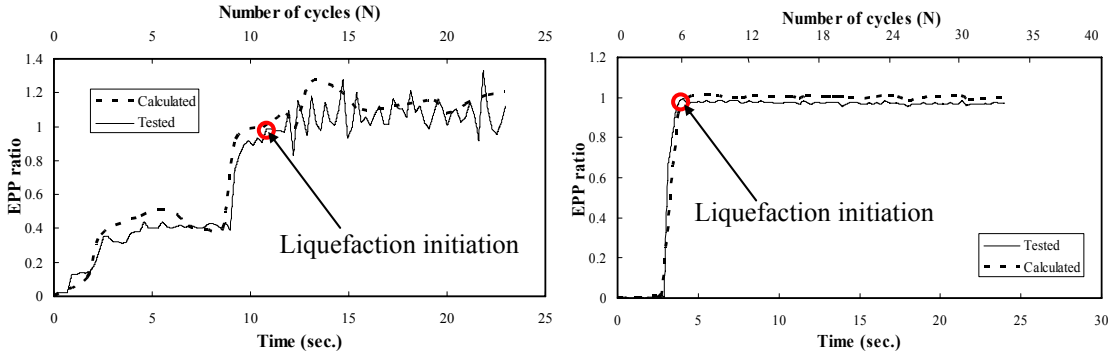

(a) Michoacan earthquake **(b) Bigbear earthquake**

Figure 6. Tested and calculated EPP ratio curves for earthquake loading tests

CONCLUSION

When a dynamic force such as earthquake is applied to saturated sand, the EPP builds up continuously with decreases of sand strength and sands are eventually liquefied. In this paper, for the analysis of dynamic soil behavior under undrained loading conditions, an EPP generation model was developed for better simulation of dynamic responses for saturated sands. To predict EPP using the proposed model, calculated results based on the proposed model were compared with those from additional experimental tests. Results of the prediction showed good agreement with tested results until the initial liquefaction. From results of the prediction, it was found that the proposed model describe reasonably well the EPP-dissipated energy responses for various types of irregular earthquake loadings.

ACKNOWLEDGEMENTS

This work has been supported by Yonsei University, Center for Future Infrastructure System, a Brain Korea 21 program, Korea.

REFERENCES

Abrahamson, N., and Silva, W. Empirical ground motion models, Draft Report. Brookhaven National Laboratory, 1996

Arias, A. Measure of earthquake intensity, R. J. Hansen, ed. Seismic Design for Nuclear Power Plants, The M. I. T. Press, Cambridge, Mass, 1970

Dobry, R., Ladd, RS., Yokel, FY., Chung, RM., and Powell, D. Prediction of pore water pressure buildup and liquefaction of sands during earthquakes by the cyclic strain method, NBS Building Science Series 138, US Department of Commerce, 152p., 1982

Elenas, A., and Liolios, A. “Earthquake induced nonlinear behavior of reinforced concrete frame structures in relation with characteristic acceleration parameters,” *Proc. of the 5th International Conference on Seismic Zonation,* Quest editions, Vol. II, Presses Academiques, Nantes, 1013-1020, 1995

Green, RA. Energy based evaluation and remediation of liquefiable soils, Ph.D. Dissertation, Virginia Polytechnic Institute and State University, 397p., 2001

Green, RA., Mitchell, JK., and Polito, CP. “An energy based excess pore pressure generation model for cohesionless soils,” *Proc.: Developments in Theoretical Geomechanics – The John Booker Memorial Symposium* (D. W. Smith and J. P. Carter, eds), Sydney, New South Wales, Australia, Nov. 16-17, A. A. Balkema Publishers, Rotterdam, Netherlands, 383-390, 2000

Ishihara, K., and Yasuda, S. “Sand liquefaction due to irregular excitation,” *Soils and foundation*, 12(4), 65-77, 1972

Ishihara, K. and Yasuda, S. “Sand liquefaction in hollow cylinder torsion under irregular excitation,” *Soils and foundation*, 15(1), 45-59, 1975

Kramer, S.L., and Mitchell, R.A. “Ground motion intensity measures for liquefaction hazard evaluation,” *Earthquake Spectra,* Volume 22, Issue 2, 413-438, 2006

Kramer, S. L., Jones, A. A., Everhard, M. O., and Arduino, P. Seismic instrumentation for the Alaskan way viaduct, WA-RD 520.1. Washington State Department of Transportation, 2002

Kim, S. I. “Liquefaction potential in moderate earthquake regions,” *Proc. of the 12th Asian Regional Conf. on Soil Mech. And Geo. Eng.,* Leung, C. F., Phoon, K. K., Chow, Y. K., Teh, C. I., and Yong, K. Y. editions, Vol. II, World Scientific, Singapore, 1109-1138, 2003

Kim, SI., Park, KB., Park, SY., Hwang, SJ., Lee, JH., and Choi, JS. “Effects of irregular dynamic loads on soil liquefaction,” *16th International Conference on Soil Mechanics and Geotechnical Engineering*, Osaka, Vol. 4, 4b, 2673-2676, 2005

Ladd, R. S. “Preparing test specimens using under compaction,” *Geotechnical Testing Journal.*, 1(1), 16-23, 1978

Law, KT., Cao, YL., and He, GN. “An energy approach for assessing seismic liquefaction potential,” *Canadian Geotechnical Journal*, Vol. 27, 320-329, 1990

Liang, L. Figueroa, JL., and Saada AS. “Liquefaction under random loading: unit energy approach,” *Journal of Geotechnical Engineering*, 121(11), 776-781, 1995

Meskouris, K., Kraitzig, W. B., and Hanskotter, U. “Nonlinear computer simulations of seismically excited wall-stiffened reinforced concrete buildings,” *In Structural Dynamics EUROD YN '93, ed. Moan et al*., Balkema, Rotterdam, 49-54, 1993

Nemat-Nasser, S., and Shokooh, A. “A unified approach to densification and liquefaction of cohesionless sand in cyclic shearing,” *Canadian Geotechnical Journal.*, Ottawa, 16, 659-678, 1979

Park, IJ. Disturbed state modeling for dynamic and liquefaction analysis, PhD. Thesis, Dept. of CEEM, Univ. of Arizona, AZ, USA, 1997

Seed, HB., and Idriss, IM. “Simplified procedure for evaluating soil liquefaction potential,” *Journal of the Soil Mechanics and Foundations Division*, 97(SM9), 1249-1273, 1971

Simcock, KJ., Davis RO., Berrill, JB., and Mullenger G. “Cyclic triaxial tests with continuous measurement of dissipated energy,” *Geotechnical Testing Journal*, 6(1), 35-39, 1983

Tao, M. Case history verification of the energy method to determine the liquefaction potential of soil deposits, Ph.D. Dissertation, Case Western Reserve University, 2003

Trifunac, M. D., and Novikova, E. I. “State of the art review on strong motion duration,” *Proc. of the 10th European Conference on Earthquake Engineering,* ed. G. Duma, Vol. I, Balkema, Rotterdam, 131-140, 1994

Vasquez-Herrera, A., and Dobry, R. The Behavior of Undrained Contractive Sand and Its Effects on Seismic Liquefaction Flow Failures of Earth Structures, Contract No. 86-003, Dept. of Army, U.S. Army Corps of Engineers, Washington, D.C, 1989

Weibull, WA. “A statistical distribution function of wide applicability,” *Journal of Applied Mechanics*, 18, 293-297, 1951